Research Article

Xiaohui Wang, Longsheng Wang*, Shouyun Hu, Ge Yu, Qing Wang, Zhenhua Zhang, Mingming Ma, Mengna Liao, and Lei Gao

East Asian monsoon during the past 10,000 years recorded by grain size of Yangtze River delta

https://doi.org/10.1515/geo-2020-0251
received January 18, 2020; accepted April 16, 2021

Abstract: Paleoenvironmental research is critical for understanding delta evolution processes and managing delta sustainability, particularly for delta experiencing significant recent fluvial sediment discharge. Based on other previously reported optically stimulated luminescence (OSL) data, Holocene environmental changes of the Yangtze River delta in response to climate fluctuations and human activities were reviewed on the basis of grain-size analyses of core YZ07. The results of grain-size and end-member analysis (EMA) provide a detailed history of East Asian monsoon variability and environmental changes since ~10,000 cal year B.P. The lower median values (Md) and sand content reflect relatively cool and dry climate conditions between 10,000 and 9,570 cal year B.P. During the early Holocene (9,570–7,630 cal year B.P.), the highest Md values and sand contents and the lowest end member 2 (EM2) contents suggest the Holocene transgression. The increased Md values and sand contents indicate that the climate conditions were warm and wet during the mid-Holocene thermal optimum. From 4,690 to 4,150 cal year B.P., the climate was cool and dry, corresponding to the cool event, as indicated by the finer grain size. Subsequently, between 4,150 and 2,850 cal year B.P., the grain size derived from the Md value and sand content increased, which reflect a wet and warm episode. The climate, which shifted from warm and wet to cool and dry between 2,850 and 1,020 cal year B.P., may have caused a reduction in the sand contents and Md values. After 1,020 cal year B.P., the lowest values of Md and Standard deviation (Sd) and the highest contents of EM2 and clay suggest that the Yangtze River delta has been severely affected by anthropogenic activity. The variability of the East Asian monsoon intensity in the Yangtze River delta strongly correlates with other East Asian monsoon paleoclimate records in China. These results are important for investigations into the interactions between regional systems and global change in monsoonal climatic regions and can provide an example of the evolution of a large scale geomorphic feature resulting from river-sea interaction.

Keywords: Yangtze River delta, grain size, end-member modeling analysis, East Asian monsoon

1 Introduction

Yangtze River delta is located in eastern China (122°30′ N–120°N, 32°30′E–29°30′E), and the elevations of Yangtze River delta range from 3 to 5 m above average sea level [1,2]. Yangtze River delta is highly vulnerable to typhoons, flooding, and high tides. The current dominant climate of the Yangtze River delta is the widespread East Asian monsoon (EAM), which is characterized by cold and dry during the winter and hot and wet during the summer. The EAM is a significant part of the global climatic system and plays an important role in the global hydrologic cycles [3]. The research of past monsoonal climatic history is necessary for predicting the climate changes in monsoonal areas in the near future.

Since the 1970s, a large number of research projects have been conducted in the reconstruction of the stratigraphic framework in Yangtze River delta to elucidate the relationships between the delta's evolution and paleoenvironmental change [4–15]. Grain-size distributions can be used to infer the sedimentary processes and the provenance and determine the paleo-depositional environment

* **Corresponding author: Longsheng Wang,** Coast Institute of Ludong University, Yantai 264025, China; CAS Key Laboratory of Coastal Environmental Processes and Ecological Remediation, Yantai Institute of Coastal Zone Research, Chinese Academy of Sciences, Yantai 264003, China; State Key Laboratory of Loess and Quaternary Geology, Institute of Earth Environment, Chinese Academy of Sciences, Xi'an 710061, China, e-mail: 52wls@163.com
Xiaohui Wang, Qing Wang, Zhenhua Zhang: Coast Institute of Ludong University, Yantai 264025, China
Shouyun Hu, Ge Yu, Mengna Liao, Lei Gao: State Key Laboratory of Lake Science and Environment, Nanjing Institute of Geography and Limnology, Chinese Academy of Sciences, Nanjing 210008, China
Mingming Ma: Institute of Geography, Fujian Normal University, Fuzhou 350007, China

and the sediment transport pathways [16–29]. Many grain-size proxies including sorting coefficient (or standard deviation), median grain size, kurtosis, skewness, and grain-size ratios have been shown to reflect different transport dynamics [30–34]. For example, median values (Md) are usually related to the average strength of the transport mechanics. Standard deviation (Sd) is often used as the quantification of the grain-size populations. Skewness (Sk) is a slanting asymmetry in the abnormal distribution that reflects the changes of the grain-size distribution. Kurtosis (Kg) describes the shape of a probable distribution reflecting the changes of sedimentation dynamics. However, all these grain-size parameters are not solely associated with a single process, but always represent a mixture of different transport and sedimentation dynamics.

Generally, two methods can be applied to differentiate the mixing of different processes. The first method is based on the visual particle-size distribution curves (histograms). However, the analysis of multimodal distributions is qualitative and is only useful when they are sufficiently different from individual subgroups [35]. The second method is end-member analysis (EMA). EMA does not require any specific assumptions, which suggests that the numbers and shapes of end members also are not specified, so it should be especially well suitable for separating the grain-size distributions based on principal component analysis, factor rotation, a nonnegative least-square estimation, and variable data scaling [36–39].

In this study, based on the previously reported optically stimulated luminescence (OSL) data, we systematically investigated the basic grain-size proxies and the EMA results of Holocene sediments in Yangtze River delta. First, we report variations in the grain-size parameters with age. Then, we discuss the responses of the sediment grain size to the climate fluctuations and human activities since 10,000 cal year B.P. We also address the possible driving forces of the variability of the Holocene monsoon intensity. The results can reveal the provenance and sedimentary dynamics of different sediments types since 10,000 cal year B.P. and understand the paleoenvironmental information from the sediments.

2 Regional setting

The Yangtze River originated from the Qinghai-Tibet Plateau and flowed to the East China Sea at approximately 31.5°N (Figure 1). The Yangtze River delta with approximately 51,800 km^2 has a funnel-shaped

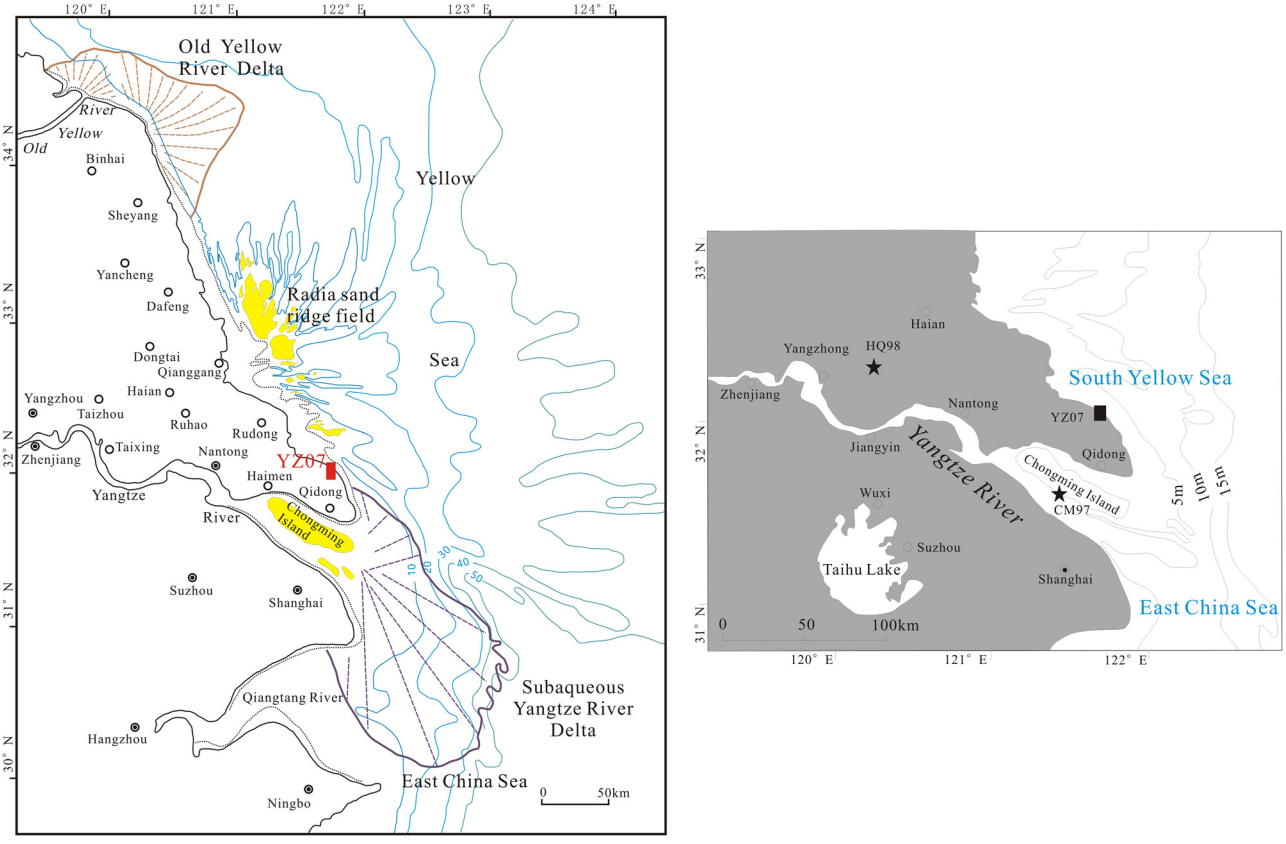

Figure 1: Distribution of Holocene deposits over the eastern China sea region (modified from ref. [69]) (left), the location of the study core YZ07, and the correlation core CM97, HQ98 in the Yangtze River delta (right).

topography and is characterized as a typical tide-dominated delta [41–45].

The current climate of the Yangtze River delta is humid subtropical climate and is largely dominated by the EAM. The annual average temperature is 15.6°C. The area is dominated by a subtropical high pressure system during the summer and experiences warm, moist conditions with a monthly average daily maximum temperature of 28.9°C. The region is under the influence of the Mongolian high pressure system during the winter and experiences cold, drought conditions with a minimum temperature of approximately 2°C. Average precipitation is approximately 1,100 mm/year, and approximately 40–45% of falls occur in the summer [40,45].

During the Last Glacial Maximum, the coastline was about 130 m below the current sea level, and most of the continental shelf in the East China Sea was subaerial [2,56]. A huge incised river valley formed in the modern Yangtze River delta during the Last Glacial Maximum [41–43]. However, with the rising of the sea level, the incised valley was submerged and then formed a tide-dominated estuary [46]. When the Holocene transgression reached the maximum during 8,500–7,000 cal year B.P., a funnel-shaped paleo-Yangtze River estuary formed in the incised valley. This river mouth was 60–90 m deep and 60–70 m wide extending from Zhenjiang–Yangzhou to the modern estuary [41,44]. Subsequently, most of the incised river valley was filled, and the current Yangtze River delta sediments were washed into the estuary. The incised valley-fill sequence after the Last Glacial Maximum consists of deltaic facies, estuarine, and fluvial in descending order [42–44].

3 Materials and methods

Core YZ07 (32.08°N, 12.601°E) was taken from the Yangtze River delta (Figure 1). The total penetration depth of core YZ07 is 150 m, and the recovered length is 143.44 m. The core was split into archive and working halves. In this study, we discuss the grain-size characteristics with a segment of the core between 0 and 46.45 m. According to OSL dates of Gao et al. [47,48], the deposits between 0 and 46.45 m were accumulated since the early Holocene (Figure 3).

For grain-size analyses, a total of 484 sediment samples were collected at vertical intervals of ~10 cm between 0 and 46.45 m. All samples were pretreated by adding H_2O_2 to remove organic matter and HCl to remove carbonate, and then were measured after dispersion with 10% $(NaPO_3)_6$ with an ultrasonic treatment [49]. Grain size was measured using a Malvern Mastersizer-S laser particle-size analyzer with 100 bins ranging from 0.02 to 2,000 μm. Loss-on-ignition (LOI), which was expressed as a percentage, was determined by the weight of the samples after ovendrying at 110°C for 4 h, annealing at 550°C for 3 h, and then the samples were reweighed. Magnetic susceptibility of the samples was measured using a Bartington MS2 Magnetic Susceptibility Meter. All measurements are conducted at the State Key Laboratory of Lake Science and Environment, Nanjing Institute of Geography and Limnology.

4 Results

4.1 Sedimentary units of core YZ07

Gao et al. [47,48] have recognized three sedimentary facies including intertidal flat, lower intertidal to subtidal

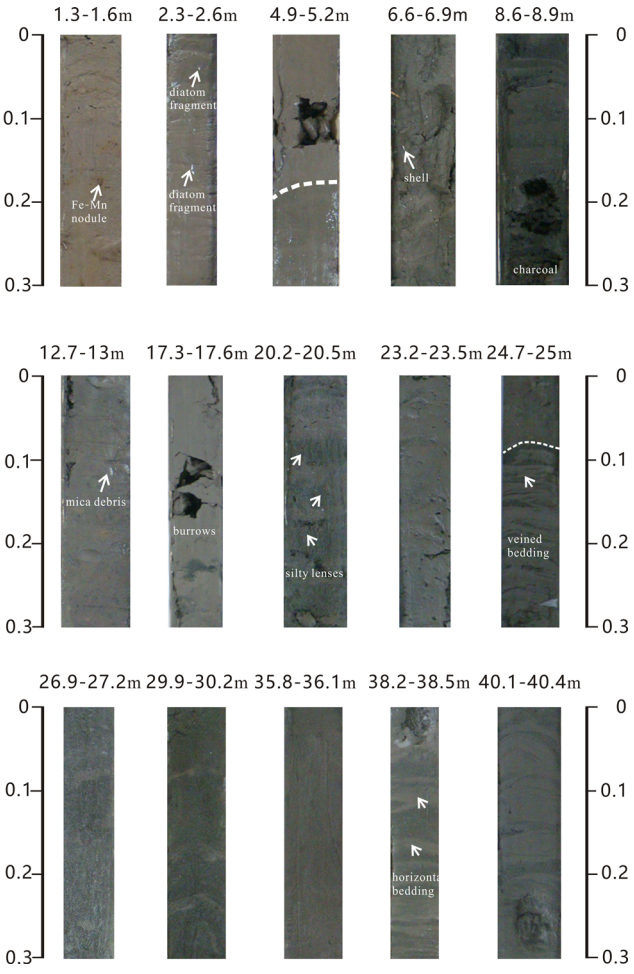

Figure 2: The lithology characteristics of typical sedimentary facies of core YZ07.

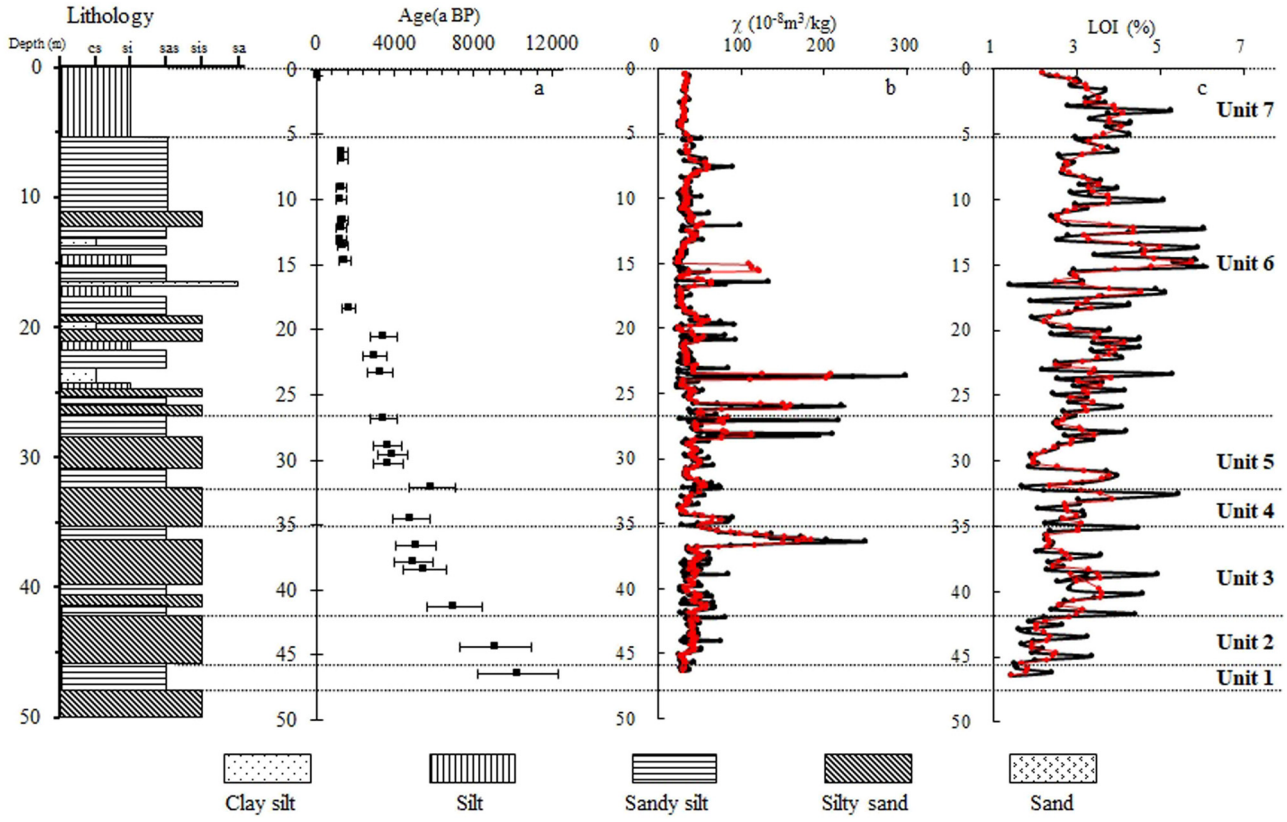

Figure 3: Values of magnetic susceptibility (b) and loss-on-ignition (c) of core YZ07, which was dated using the (a) optically stimulated luminescence method [65].

flat, and flood plain (Figure 2). In this study, according to differences in lithology, biological indicators, magnetic susceptibility (χ), and LOI, we have identified seven units for better studying the changes of grain size. Magnetic susceptibility (χ) was determined by the overall concentrations of magnetic minerals, and LOI is an index that reveals an enrichment of organic matter in the sediment sequence. Unit 1 (46.45–45.15 m; 10,000–9,570 cal year B.P.) is dominated by olive grey silty sand (Figure 2). Values of χ range from 26.87 to 44.49 $\times 10^{-8}$ m^3/kg with a mean of 28.91 $\times 10^{-8}$ m^3/kg. Values of LOI range from 1.42 to 2.41% with a mean of 1.78%. Unit 2 (45.15–42.17 m; 9,570–7,630 cal year B.P.) mainly consists of grey sandy silt (Figure 2). Values of χ range from 25.16 to 81.14 $\times 10^{-8}$ m^3/kg with a mean of 42.93 $\times 10^{-8}$ m^3/kg. Values of LOI range from 1.60 to 3.36% with a mean of 2.23%. Unit 3 (42.17–34.47 m; 7,630–4,690 cal year B.P.) is made up of dark grey sandy silt and silty sand (Figure 2). Values of χ range from 26.73 to 249.96 $\times 10^{-8}$ m^3/kg with a mean of 62.53 $\times 10^{-8}$ m^3/kg. Values of LOI range from 2.05 to 4.93% with a mean of 2.93%. Unit 4 (34.47–32.40 m; 4,690–4,150 cal year B.P.) is dominated by light brown silty sand (Figure 2). Values of χ range from 25.37 to 56.75 $\times 10^{-8}$ m^3/kg with a mean of 35.79 $\times 10^{-8}$ m^3/kg. Values of LOI range from 2.06 to 5.43% with a mean of 3.23%. Unit 5 (32.40–24.64 m; 4,150–2,850 cal year B.P.) mainly consists of light brown silty sand and sandy silt (Figure 2). Values of χ range from 26.70 to 221.33 $\times 10^{-8}$ m^3/kg with a mean of 56.78 $\times 10^{-8}$ m^3/kg. Values of LOI range from 1.67 to 4.17% with a mean of 2.79%. Unit 6 (24.64–4.99 m; 2,850–1,020 cal year B.P.) is made up of light brown clayey silt, sand silt, silt, silty sand, and sand (Figure 2). Values of χ range from 22.29 to 297.97 $\times 10^{-8}$ m^3/kg with a mean of 40.79 $\times 10^{-8}$ m^3/kg. Values of LOI range from 1.39 to 6.06% with a mean of 3.47%. Unit 7 (4.99–0 m; 1020 cal year B.P.-present) is dominated by light olive grey silt (Figure 2). Values of χ range from 25.49 to 38 $\times 10^{-8}$ m^3/kg with a mean of 32.65 $\times 10^{-8}$ m^3/kg. Values of LOI range from 2.17 to 5.26% with a mean of 3.44% (Figure 3). The results of χ and LOI supported the seven units of the core YZ07 between 0 and 46.45 m.

4.2 Grain-size parameters

The mean Md value in core YZ07 is 52.66 μm (Figure 4). The highest and lowest values occurred at depths of

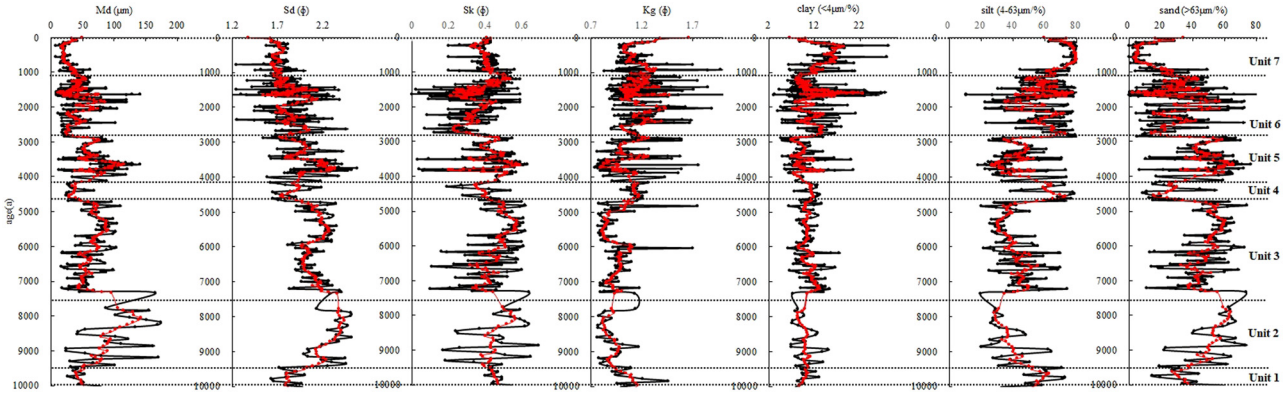

Figure 4: Grain-size parameters including Md, Sd, SK, Kg and the contents of clay, silt, and sand against age for each unit (black lines are the original values, with red lines smoothed by a 5-point running average).

42.17–45.15 m (mean, 94.28 μm) and 0–4.99 m (mean, 23.78 μm), respectively. The mean Sd, Sk, and Kg values are 1.93, 0.41, and 1.08, indicating medium sorting, positive skewness, and medium kurtosis. The mean clay content (0–4 μm) is 11.07%. The highest and lowest contents occurred at depths of 0–4.99 m (mean, 14.73%) and 24.64–32.40 m (mean, 9.14%), respectively. The mean silt content (4–63 μm) is 52.07%. The highest and lowest contents occurred at depths of 0–4.99 m (mean, 76.51%) and 42.17–45.15 m (mean, 38.00%), respectively. The mean sand content (>63 μm) is 36.23%. The highest and lowest contents occurred at depths of 42.17–45.15 m (mean, 52.36%) and 0–4.99 m (mean, 8.77%), respectively (Figure 4, Table 1). Sedimentary facies from the results of grain size were consistent with the χ and LOI.

The typical grain-size distributions of core YZ07 are illustrated in Figure 5. The curve shapes of the grain-size distribution of units 1, 2, 3, and 5 show two peaks and are clearly shifted to the sand side, with the main peaks occurring at 100, 250, 160, and 158 μm, respectively. The curve of Unit 6 shifted to coarse silt and shows two peaks occurring at 55 and 12 μm. The curves of units 4 and 7 show a single peak. The main peak occurred at 45 and 11 μm, respectively. All those show the sediments of unit 1, 2, 3, and 5 are coarest, and the sediments of unit 4 and 7 are finest.

4.3 Grain-size end-member analysis

Using AnalySize Software as proposed by Paterson and Heslop [50] to demonstrate the applicability of EMA, we calculated the squared linear correlation (R^2) and angular distance in degrees (theta) by assuming two to seven end members. Figure 6a and b show that the grain-size data

Table 1: Comparison of the range and mean value of grain-size parameters during different units

Sample	Values	Md (μm)	Sd (ϕ)	Sk (ϕ)	Kg (ϕ)	Clay (<4 μm/%)	Silt (4–63 μm/%)	Sand (>63 μm/%)
Unit 1	Range	27.08–106.03	1.63–2.35	0.18–0.58	0.77–1.52	6.04–14.20	25.14–72.59	14.36–68.81
	Mean	55.32	1.93	0.44	1.07	9.15	48.45	42.40
Unit 2	Range	23.70–173.89	1.72–2.51	0.17–0.69	0.76–1.17	6.84–14.96	19.69–70.31	19.05–73.11
	Mean	94.28	2.25	0.46	0.91	9.63	38.00	52.36
Unit 3	Range	16.23–109.60	1.81–2.40	0.10–0.62	0.77–1.75	6.13–17.35	19.97–73.32	11.04–73.61
	Mean	64.31	2.11	0.46	0.93	10.72	40.76	48.52
Unit 4	Range	24.22–95.44	1.59–2.18	0.19–0.60	0.86–1.43	7.62–13.14	28.52–78.66	8.65–62.38
	Mean	40.03	1.85	0.40	1.14	10.92	63.25	25.83
Unit 5	Range	12.97–140.66	1.54–2.57	0.03–0.63	0.74–1.76	4.53–20.38	18.15–73.13	6.49–76.33
	Mean	73.69	2.06	0.45	1.02	9.14	39.33	51.53
Unit 6	Range	8.35–140.91	1.15–2.45	0–0.59	0.83–2.46	3.03–27.52	10.68–83.61	0.29–86.16
	Mean	40.30	1.83	0.37	1.17	11.84	59.69	28.47
Unit 7	Range	8.01–48.57	1.25–1.82	0.20–0.47	0.96–1.70	6.31–28.20	59.54–83.24	0.02–33.99
	Mean	23.78	1.69	0.39	1.14	14.73	76.51	8.77

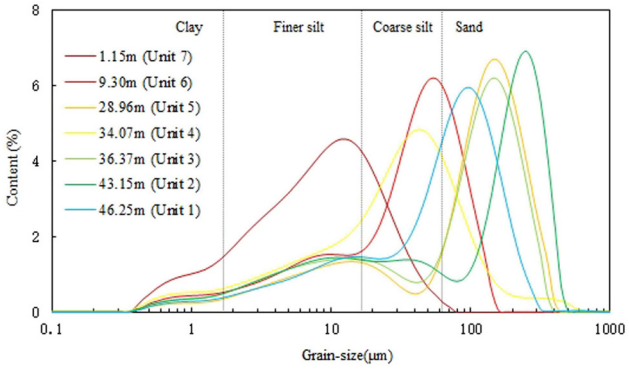

Figure 5: Grain-size distribution frequency curves of the representative samples from the core YZ07 in the Yangtze River delta.

can best be explained by a 5-end-member model. More end members will not provide a better explanation of the dataset as R^2 does not increase much. Adding more end member will increase noise [51,52].

Each end member (EM) has a dominant peak and presents normal grain-size distribution curves for the five EMs (Figure 6c). With the increasing of the grain size of the dominant peak, the sorting improves toward coarse grains from EM1 to EM5. EM1 has a mode of 14 μm, with a majority in the finer silt range, indicating that EM1 is typically transported as suspension. EM2 has a mode of 35 μm, with a majority in the coarse silt range, which show that EM2 could behave as either semi-suspension or bedload depending on hydrodynamic conditions. So EM2 can be more sensitive for hydrodynamic conditions caused by climate changes. EM3 has a mode of 71 μm, with a majority in the very fine sand range. The mode of EM4 is 142 μm, and it is mainly distributed in the fine sand. EM5 has a mode of 252 μm, most within the sand range. The sub-peaks of EM3, EM4, and EM5 are lower in the range of fine silt, indicating that EM3, EM4, and EM5 can be transported by saltation [39,41].

Figure 7 and Table 2 show the distribution of the relative contents of the five EMs, which range from 0 to 100%. The mean content of EM1 is 27.26%. The highest and lowest values occurred at depths of 0–4.99 m (36.05%) and 42.17–45.15 m (21.59%), respectively. The mean content of EM2 is 21.23%. The highest and lowest values occurred at depths of 0–4.99 m (50.28%) and 42.17–45.15 m (8.43%), respectively. The mean content of EM3 is 23.28%. The highest and lowest values occurred at depths of 45.15–49.93 m (31.57%) and 0–4.99 m (11.10%), respectively. The mean content of EM4 is 20.60%. The highest and lowest values occurred at depths of 34.47–42.17 m (39.97%) and 0–4.99 m (0.46%), respectively. The mean content of EM5 is 7.09%. The highest and lowest values occurred at depths of 42.17–45.15 m (33.87%) and 0–4.99 m (0.02%), respectively.

5 Discussion

Grain-size analyses from sediments of core YZ07 from the Yangtze River delta provide the detailed paleoenvironmental evolutional history since 10,000 cal year B.P.

5.1 Unit 1 (10,000–9,570 cal year B.P.)

Data from the $\delta^{13}C$ record of the Hani Peat from the Northeast China [53], the $\delta^{18}O$ record of Dongge Cave from the eastern China [54], and the redness record of Qinghai Lake from the Northwest China [55] have been attributed to a relatively cool and drought condition from 10,000 to 9,570 cal year B.P. (Figure 8), and the pollen assemblages from the Yangtze River delta also suggest dry and cool conditions [8,9,25]. In core YZ07, the lower

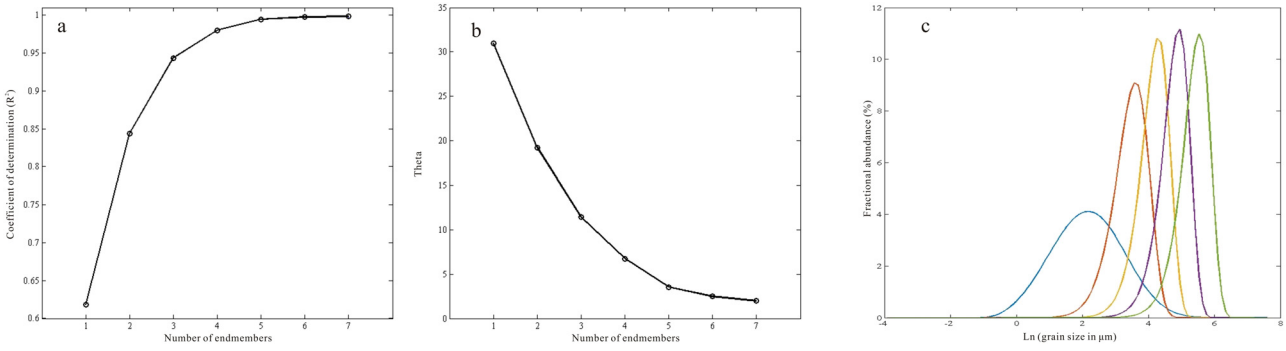

Figure 6: EMA results of the grain-size data from YZ07 in the Yangtze River delta. (a) The squared linear correlation (R^2). (b) The angular distance in degrees (Theta). (c) Grain-size distribution for each end-member.

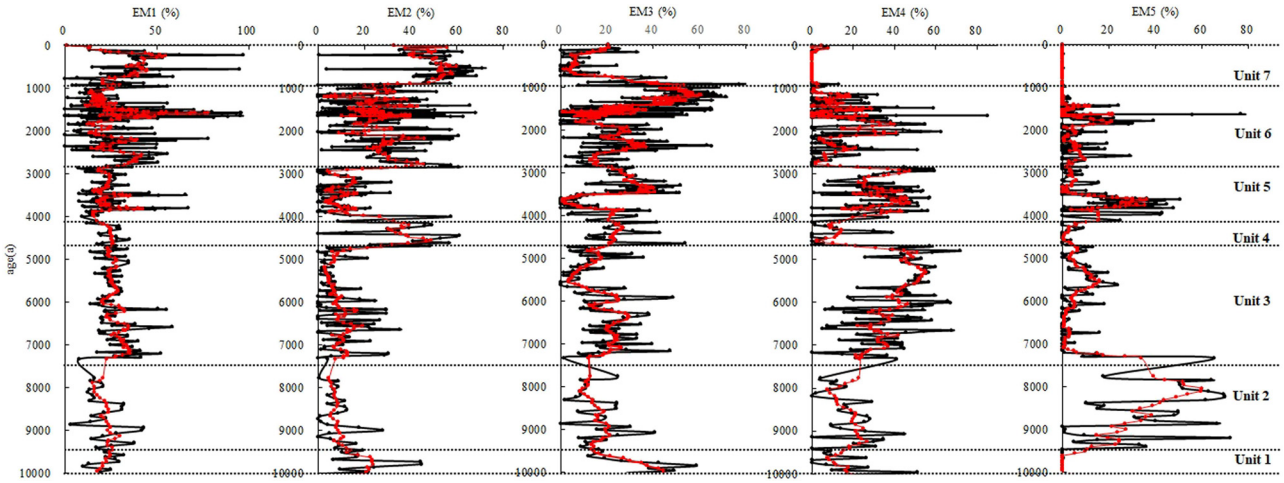

Figure 7: Temporal distributions of the relative contents of the five EMs of the sediments from core YZ07 in the Yangtze River delta.

Table 2: Comparison of the range and mean value of EMMA results during different units

Sample	Values	EM1 (%)	EM2 (%)	EM3 (%)	EM4 (%)	EM5 (%)
Unit 1	Range	9.50–36.50	0–44.68	5.43–58.73	0–53.42	0–22.66
	Mean	21.50	15.85	31.57	26.01	3.77
Unit 2	Range	3.32–42.70	0–27.75	0–40.54	0–44.81	0–72.25
	Mean	21.59	8.43	14.86	17.58	33.87
Unit 3	Range	13.79–58.30	0–35.35	0–48.43	0–71.70	0–23.86
	Mean	28.17	8.83	17.57	39.97	5.45
Unit 4	Range	9.40–35.15	0–61.03	3.27–53.86	0–57.16	0–24.87
	Mean	23.35	37.77	24.35	11.11	3.42
Unit 5	Range	7.40–66.96	0–31.57	0–51.79	0–59.64	0–50.60
	Mean	23.30	8.91	19.46	34.78	13.56
Unit 6	Range	0–95.88	0–67.87	0–80.71	0–85.03	0–76.93
	Mean	29.14	26.19	29.01	11.88	3.77
Unit 7	Range	0–9.71	0.55–71	0–45.72	0–7.74	0–0.51
	Mean	36.05	50.28	11.10	0.46	0.02

Md values, higher EM2 contents, and lower Sd values indicate that the grain size of sediments decreased in this section. During 10,000 to 9,570 cal year B.P., rainfalls in the Yangtze River valley decreased leading to weaker hydrodynamic conditions [58]. Weak hydrodynamic conditions brought the fine-grained sediments to the study area.

5.2 Unit 2 (9,570–7,630 cal year B.P.)

At around 9,570–7,630 cal year B.P., the highest values of Md and Sd suggest strong hydrodynamic conditions, which is also supported by the lowest EM2 contents. The previous studies indicate that the Holocene transgression reached the maximum in 7,000–8,500 cal year B.P. [41–44]. The Holocene transgression has made the study area to be depocenter [5]. More and coarser sediments were brought to the study area. These resulted in the rapid increase of Md and Sd values and the decrease of EM2 contents.

5.3 Unit 3 (7,630–4,690 cal year B.P.)

The grain-size records of this period show a mean Md value of 64.31 μm and a mean clay content of 10.72%. These data indicated that from 7,630 to 4,960 cal year B.P., the East Asian monsoon remained strong in the Yangtze River delta region. The pollen assemblages are comparable to those found in various parts of China which were interpreted as reflecting mid-Holocene hypsithermal conditions. In other palynological studies in the

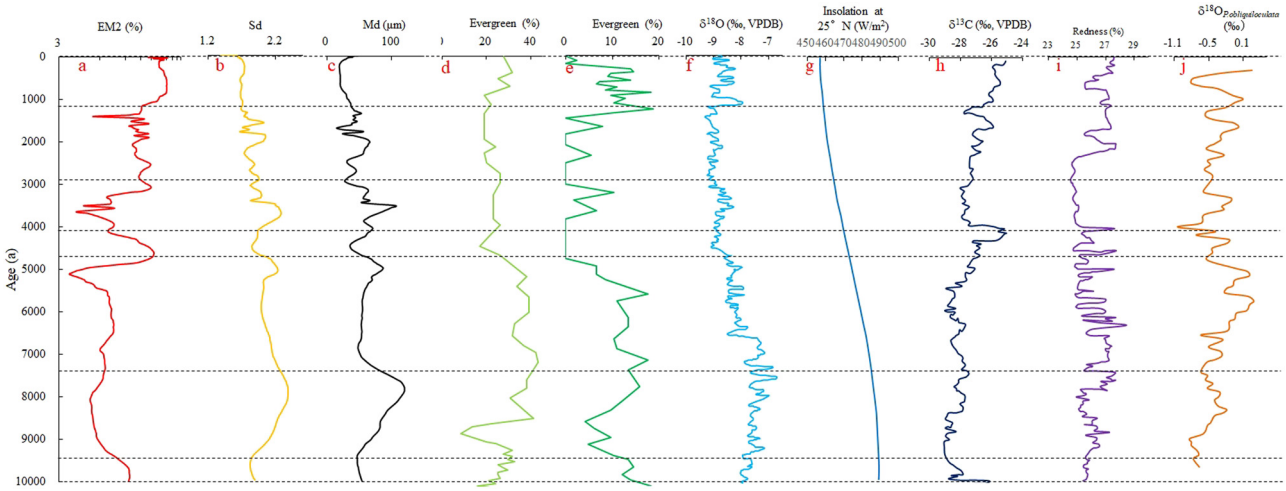

Figure 8: (a) EM2 values, (b) Sd values, and (c) Md values smoothed by 5-point running averages for core YZ07. (d) The changes of evergreen of core CM97 from Yangtze River delta [8,9] (e) The changes of evergreen of core HQ98 from Yangtze River delta [8–10] (f) Stalagmite $\delta^{18}O$ record from Dongge Cave [49]. (g) NH summer solar insolation at 45oN [66]. (h) Cellulose $\delta_{13}C$ record from Hani Peat [55]. (i) Redness data from Qinghai Lake [50]. (j) Sea surface temperature reconstructed on the Mg/Ca ratio of Globigerinoides ruber from MD81 core in the western tropical Pacific [63].

lower reaches of the Yangtze delta region, the average temperature during 7,630–4,960 cal year B.P. was 2–4°C warmer than that of today [44].

The grain-size data suggested that the climate of most areas in the northeastern and central China was wetter and warmer than that at the present [58]. The wet and warm conditions in the central and northeastern China suggested the increasing influence of the mid-Holocene Pacific monsoon [59]. From 7,632 to 4,837 cal year B.P., the pollen assemblages in the Yangtze River delta, the $\delta^{18}O$ record of Dongge Cave from the eastern China [60], the $\delta^{13}C$ record of the Hani Peat from the Northeast China, and the redness record of Qinghai Lake from the Northwest China all reached the highest levels since the Holocene, indicating that climate in these regions is warmest and wettest. An concluded that the optimal climatic conditions in the middle and lower reaches of the Yangtze river were found at about 6,000 cal year B.P. using the numerical simulation of east Asian monsoon season cycle [3].

5.4 Unit 4 (4,690–4,150 cal year B.P.)

A cool and dry climate was shown from 4,690 to 4,150 cal year B.P. by an abrupt reduction in Md and a rapid increase of EM2 contents. The cool and dry climatic conditions caused weak hydrodynamic conditions. Climatic cooling events between 4,700 and 3,500 cal year B.P. have been reported in many parts of the world [61,62]. In China, Liu et al. [56] reported that the lower reaches of the Yangtze River began to become cool after approximately 4,400 cal year B.P. followed by a warmer and wetter low temperature event in the middle Holocene. Ice wedges found in Yitulihe of the northeastern China that formed between 4,500 and 3,000 cal year B.P. indicate a bitterly cold Neoglacial period [64,65]. A similar cooling trend was shown in many areas of China, where pollen data during the middle and late Holocene were recorded [8,9,66,67]. The cool and dry climatic period recorded by core YZ07 is different from the above results. The reason for this may be that chronological uncertainties such as differences of dating methods are likely to have affected the recorded patterns of climatic change on a multi-millennium time scale.

5.5 Unit 5 (4,150–2,850 cal year B.P.)

The increase of Md value, sand content, and the decrease of clay and EM2 content indicated the arrival of warm and humid episodes. However, this time period belongs to the Neoglacial period, which is also suggested by the increase of deciduous trees and subtropical evergreen such as *Quercus* (*Lepidobalanus*), *Quercus* (*Cyclobalanopsis*), *Morus*, *Ulmus/Zelkova*, and *Castanopsis/Lithocarpus* from cores HQ98 and CM97 in the Yangtze River delta. The low frequencies of conifers from cores HQ98 and CM97 also suggested that the climate conditions were warm and humid during this period [8,9,67].

5.6 Unit 6 (2,850–1,020 cal year B.P.)

As shown by an increase in EM2 and clay contents, a cool climatic stage occurred during 2,850–1,020 cal year B.P. A cool climatic phase occurred at this time, as suggested by an increase in the occurrence of conifers including *Pinus* and *Fagus* along with rare subtropical broadleaved evergreen and deciduous broadleaved trees from cores HQ98 and CM97 in the Yangtze River delta [44]. The shift from warm and humid to cool and dry climate may result in a decrease of the sand contents and Md values. Chen et al. [69] have reviewed the historical document of China and recorded that the climatic conditions in the lower reaches of the Yangtze river during the Northern and Southern dynasties (about AD 350–580) were so cold that rivers and lakes were frozen in the winter. Based on a study of peat cellulose, Hong et al. [55] recognized a significant decrease of the temperature from about 1,800 to 1,600 cal year B.P. This cooling process is consistent with the Kofun cooling period recorded in Japan (AD 240–732) [68–69]. The redness record of northwest part of Qinghai lake [57] and the declining abundance of *Pulleniatina obliquiloculata* in the northwest Pacific Ocean [70] can also be used to infer cold and dry periods.

5.7 Unit 7 (1,020 cal year B.P.-present)

During this period, the grain size shows the lowest Md values and the highest EM2 and clay contents. The lowest values χ and the highest LOI values also imply a significant increasing of aquatic productivity [71]. We hypothesized that those could be influenced by the enhancement of human impacts such as industry, agriculture, deforestation, and soil erosion. Human activities resulted in strong agitations of land surface, which can lead to a sharp decrease in the Md value and abrupt increase in the EM2 and clay contents.

6 Conclusion

Based on the grain-size parameters of core YZ07 from the Yangtze River delta and a time control provided by a number of OSL ages, past changes of the EAM climate and sedimentary environment have been deduced using sediment grain-size analysis method of end-member model.

Between 10,000 and 9,570 cal year B.P., the climate of the Yangtze River delta was cool and dry as indicated by the lower Md values and sand contents. During the early Holocene (9,570–7,630 cal year B.P.), the highest Md value and sand content and lowest EM2 contents suggest a Holocene transgression. The climate during the mid-Holocene thermal optimum (7,630–4,690 cal year B.P.) was warm and wet. The strong East Asian monsoon with low seasonal variation encouraged the increase in Md and sand. From 4,690 to 4,150 cal year B.P., the climate was cool and dry, corresponding to the cool event, as indicated by the finer grain size. Subsequently, between 4,150 and 2,850 cal year B.P., the grain size derived from the Md value and sand content increased, reflecting a warm and wet episode. A cool climatic phase occurred between 2,850 and 1,020 cal year B.P., as suggested by an increase in EM2 and clay contents. The climate shifted from warm and wet to cool and dry, which may have caused a reduction of the sand contents and Md values. After 1,020 cal year B.P., the lowest values of Md and Sd and the highest contents of EM2 and clay suggest that the Yangtze River delta has been severely influenced by anthropogenic activity. The variability of EAM intensity in the Yangtze River delta is strongly consistent with other EAM paleoclimate records in China. This study not only provides a basis for Yangtze River delta paleoenvironmental reconstruction by integrating detailed logs of grain-size parameters, but also provides constraints for exploring the land-sea interactions recorded in the sediment cores as a part of the earth system, and thus, demonstrates the effectiveness of this approach.

Acknowledgments: We thank Prof. Shu Gao (East China Normal University), Prof. Yong Yin (Nanjing University), and Dr. Yongfei Li (Nanjing Institute of Geography and Limnology, Chinese Academy of Sciences) for collecting the samples. We also thank Prof. Erwin Appel (University of Tübingen) for the instructive comments.

Funding information: This research was supported financially by the National Natural Science Foundation of China (NO. 41702185, U1706220); Humanity and Social Science Foundation of Ministry of Education of China (NO. 19YJCZH171); the open foundation of CAS Key Laboratory of Coastal Environmental Processes and Ecological Remediation, YICCAS (NO.2020KGJJ10); the open foundation of State Key Laboratory of Loess and Quaternary Geology, Institute of Earth Environment, CAS (NO. SKLLQG2024); the Natural Science Foundation of Shandong Province (NO. ZR2018PD005); the Chinese Academy of Sciences Visiting Professorship for Senior International Scientists (NO. 2012T1Z0004, 131432WGZJTPYJY20150002).

Conflict of interest: Author state no conflict of interest.

References

[1] Chen Z. Geomorphology and coastline change of the Lower Yangtze delta plain, China. In: Miller AJ, Gupta A, editors. Varieties of fluvial form. New York: Wiley; 1999. p. 427–43.

[2] Saito Y, Yang Z, Hori K. The Huanghe (Yellow River) and Changjiang (Yangtze River) deltas: a review on their characteristics, evolution and sediment discharge during the Holocene. Geomorphology. 2001;41:219–31. doi: 10.1016/S0169-555X(01)00118-0.

[3] An ZS. The history and variability of the East Asian paleomonsoon climate. Quat Sci Rev. 2000;19:171–87. doi: 10.1016/S0277-3791(99)00060-8.

[4] Li CX, Li P. The characteristics and distribution of Holocene sand bodies in the Changjiang delta area. Acta Oceanol Sin. 1983;2:54–6. doi: CNKI:SUN:SEAE.0.1983-01-009.

[5] Chen ZY, Stanley DJ. Quaternary subsidence and river channel migration in the Yangtze Delta plain, eastern China. J Coast Res. 1995;11:927–45. doi: 10.1016/0025-3227(93)90158-R.

[6] Li CX, Wang P, Sun HP, Zhang JQ, Fan DD, Deng B. Late Quaternary incised-valley fill of the Yangtze delta (China): its stratigraphic framework and evolution. Sediment Geol. 2002;2:133–58. doi: 10.1016/S0037-0738(02)00066-0.

[7] Zhu C, Zheng CG, Ma CM, Yang XX, Gao XZ, Wang HM, et al. On the Holocene sea-level highstand along the Yangtze Delta and Ningshao Plain, East China. Chin Sci Bull. 2003;24:2672–83. doi: 10.1007/BF02901755.

[8] Yi SH, Saito Y, Oshima H, Zhou Y, Wei H. Holocene environmental history inferred from pollen assemblages in the Huanghe (Yellow River) delta, China: climatic change and human impact. Quat Sci Rev. 2003a;22:609–28. doi: 10.1016/S0277-3791(02)00086-0.

[9] Yi SH, Saito Y, Zhao QH, Wang PX. Vegetation and climate changes in the Changjiang (Yangtze River) Delta, China, during the past 13,000 years inferred from pollen records. Quat Sci Rev. 2003b;14:1501–19. doi: 10.1016/S0277-3791(03)00080-5.

[10] Hori K, Saito Y. An early Holocene sea-level jump and delta initiation. Geophys Res Lett. 2007;34:266–78. doi: 10.1029/2007GL031029.

[11] Zhao BC, Wang ZH, Chen J, Chen ZY. Marine sediment records and relative sea level change during late Pleistocene in the Changjiang delta area and adjacent continental shelf. Quat Int. 2008;1:164–72. doi: 10.1016/j.quaint.2007.08.006.

[12] Xu J. Response of land accretion of the Yellow River delta to global climate change and human activity. Quat Int. 2008;186:4–11. doi: 10.1016/j.quaint.2007.08.032.

[13] Xu TY, Wang GQ, Shi XF, Wang X, Yao ZQ, Yang G, et al. Sequence stratigraphy of the subaqueous Changjiang (Yangtze River) delta since the Last Glacial Maximum. Sediment Geol. 2016;331:132–47. doi: 10.1016/j.sedgeo.2015.10.014.

[14] Han TO, Win WZ, Cho CTK. Analysis of Streamflow Response to Changing Climate Conditions Using SWAT Model. Civ Eng J 6(2):194–209. doi: 10.28991/cej-2020-03091464.

[15] Fazelabdolabadi K, Golestan T. Towards Bayesian quantification of permeability in micro-scale porous structures – the database of micro networks. HighTech Innov J. 1998;1(4):148–60.

[16] Kranck K, Smith PC, Milligan TG. Grain-size characteristics of fine-grained unflocculated sediments I: 'one-round' distributions. Sedimentology. 1996a;43:589–96. doi: 10.1046/j.1365-3091.1996.d01-27.x.

[17] Kranck K, Smith PC, Milligan TG. Grain-size characteristics of fine-grained unflocculated sediments II: 'multi-round' distributions. Sedimentology. 1996b;43:597–606. doi: 10.1046/j.1365-3091.1996.d01-28.x.

[18] Passe T. Grain size distribution expressed as tanh-functions. Sedimentology. 1997;44:1011–4. doi: 10.1111/j.1365-3091.1997.tb02175.x.

[19] Prins MA, Weltje GJ. End-member modeling of siliciclastic grain-size distributions: the late Quaternary record of aeolian and fluvial sediment supply to the Arabian Sea and its paleoclimatic significance. In: Harbaugh J, et al., editors. Numerical experiments in stratigraphy: recent advances in stratigraphic and sedimentologic computer simulations. Vol. 62. SEPM (Society for Sedimentary Geology) Springer: Special Publication; 1999. p. 91–111.

[20] Sun DH. Monsoon and westerly circulation changes recorded in the late Cenozoic aeolian sequences of Northern China. Glob Planet Change. 2004;41:63–80. doi: 10.1016/j.gloplacha.2003.11.001.

[21] Chen ZY, Saito Y, Kanai Y, Wei TY, Li LQ, Yao HS, et al. Low concentration of heavy metals in the Yangtze estuarine sediments, China: a diluting setting. Estuar Coast Shelf Sci. 2004;1:91–100. doi: 10.1016/j.ecss.2003.11.021.

[22] Qin XG, Cai BG, Liu TS. Loess record of the aerodynamic environment in the East Asia monsoon area since 60,000 years before present. J Geophys Res. 2005;110:B01204. doi: 10.1029/2004JB003131.

[23] Yi L, Yu H, Ortiz JD, Xu X, Chen S, Ge J, et al. Late Quaternary linkage of sedimentary records to three astronomical rhythms and the Asian monsoon, inferred from a coastal borehole in the south Bohai Sea, China. Palaeogeogr Palaeoclimatol Palaeoecol. 2012;329–330:101–17. doi: 10.1016/j.palaeo.2012.02.020.

[24] Wang ZH, Zhan Q, Long HY, Saito Y, Gao XQ, Wu XX, et al. Early to mid-Holocene rapid sea-level rise and coastal response on the southern Yangtze delta plain, China. J Quat Sci. 2013;28(7):659–72. doi: 10.1002/jqs.2662.

[25] Amireh BS. Grain size analysis of the Lower Cambrian–Lower Cretaceous clastic sequence of Jordan: sedimentological and paleo-hydrodynamical implications. J Asian Earth Sci. 2015;97:67–88. doi: 10.1016/j.jseaes.2014.09.029.

[26] Lu Y, Fang XM, Appel E, Wang JY, Herb C, Han WX, et al. A 7.3–1.6 Ma grain size record of interaction between anticline uplift and climate change in the western Qaidam Basin, NE Tibetan Plateau. Sediment Geol. 2015;319:40–51. doi: 10.1016/j.sedgeo.2015.01.008.

[27] Zhang ZC, Dong ZB. Grain size characteristics in the Hexi Corridor Desert. Aeolian Res. 2015;18:55–67. doi: 10.1016/j.aeolia.2015.05.006.

[28] Li MK, Ouyang TP, Tian CJ, Zhu ZY, Peng SS, Tang ZH, et al. Sedimentary responses to the East Asian monsoon and sea level variations recorded in the northern South China Sea over

the past 36k year. J Asian Earth Sci. 2018. doi: org/10.1016/j.jseaes.2018.01.001.
[29] Cham DD, Son NT, Minh NQ, Thanh NT, Dung TT. An analysis of shoreline changes using combined multitemporal remote sensing and digital evaluation model. Civ Eng J. 2020;6(1):1–10. doi: 10.28991/cej-2020-03091448.
[30] Orton GJ, Reading HG. Variability of deltaic processes in terms of sediment supply, with particular emphasis on grain size. Sedimentology. 1993;40:475–512. doi: 10.1111/j.1365-3091.1993.tb01347.x.
[31] Vandenberghe J, An ZS, Nugteren G, Lu HY, Van Huissteden J. New absolute time scale for the quaternary climate in the Chinese loess region by grain-size analysis. Geology. 1997;25(1):35–8. doi: 10.1130/0091-7613(1997)0252.3.CO;2.
[32] Xiao JL, Chang ZG, Si B, Qin X, Itoh S, Lomtatidze Z. Partitioning of the grain-size components of Dali Lake core sediments: evidence for lake-level changes during the Holocene. J Paleolimnol. 2009;42(2):249–60. doi: 10.1007/s10933-008-9274-7.
[33] Xiao JL, Fan JW, Zhou L, Zhai DY, Wen RL, Qin XG. A model for linking grain size component to lake level status of a modern clastic lake. J Asian Earth Sci. 2013;69:149–58. doi: 10.1016/j.jseaes.2012.07.003.
[34] Wen RL, Qin XG, Fan JW, Xiao JL, Zhai DY. Testing the model for linking grain-size component to lake level status of modern clastic lakes. Quat Int. 2015;355:34–43. doi: 10.1016/j.quaint.2014.04.023.
[35] Vandenberghe J. Grain size of fine-grained windblown sediment: A powerful proxy for process identification. Earth-Sci Rev. 2013;121:18–30. doi: 10.1016/j.earscirev.2013.03.001.
[36] Prins MA, Vriend M, Nugteren G, Vandenberghe J, Lu HY, Zheng HB, et al. Late quaternary aeolian dust input variability on the Chinese loess plateau: inferences from unmixing of loess grain-size records. Quat Sci Rev. 2007;26:242–54. doi: 10.1016/j.quascirev.2006.07.002.
[37] Dietze E, Hartmann K, Diekmann B, IJmker J, Lehmkuhl F, Opitz S, et al. An end-member algorithm for deciphering modern detrital processes from lake sediments of Lake Donggi cona, NE Tibetan plateau, China. Sediment Geol. 2012;243(244):169–80. doi: 10.1016/j.sedgeo.2011.09.014.
[38] Dietze E, Wünnemann B, Hartmann K, Diekmann B, Jin H, Stauch G, et al. Early to mid-Holocene lake high-stand sediments at Lake Gonggi cona, Northeastern Tibetan plateau, China. Quat Res. 2013a;79:325–36. doi: 10.1016/j.yqres.2012.12.008.
[39] Dietze E, Maussion F, Ahlborn M, Diekmann B, Hartmann K, Henkel K, et al. Sediment transport processes across the Tibetan plateau inferred from robust grain-size end members in lake sediments. Clim Past. 2013b;10:91–106. doi: 10.5194/cp-10-91-2014.
[40] Jiang D. Climate on the Yangtze Delta. Beijing, China: Meteorologica Press; 1991. p. 42–75 (in Chinese).
[41] Li CX, Chen QQ, Zhang JQ, Yang SY, Fan DD. Stratigraphy and paleoenvironmental changes in the Yangtze Delta during the Late Quaternary. J Asian Earth Sci. 2000a;18:453–69. doi: 10.1016/S1367-9120(99)00078-4.
[42] Li CX, Fan DD, Zhang JQ. Late quaternary stratigraphical framework and potential environmental problems in the Yangtze River delta. Mar Geol Quat Geol. 2000b;20(3):1–7. doi: 0253-1492(2000)03-0001-07 (in Chinese, English abstract).
[43] Hori K, Saito Y, Zhao Q, Cheng X, Wang P, Sato Y, et al. Sedimentary facies and Holocene progradation rates of the Changjiang (Yangtze) delta, China. Geomorphology. 2001a;41:233–48. doi: 10.1016/S0169-555X(01)00119-2.
[44] Hori K, Saito Y, Zhao Q, Cheng X, Wang P, Sato Y, et al. Sedimentary facies of the tide-dominated paleo-Changjiang (Yangtze) estuary during the last transgression. Mar Geol. 2001b;177:331–51. doi: 10.1016/S0025-3227(01)00165-7.
[45] Academia Sinica. Physical geography of China: climate. Beijing: Academic Press; 1985. p. 262 (in Chinese).
[46] Uehara K, Saito Y, Hori K. Paleotidal regime in the Changjiang (Yangtze) estuary, the East China Sea, and the Yellow Sea at 6 and 10 ka estimated from a numerical model. Mar Geol. 2002;183:179–92. doi: 10.1016/S0025-3227(01)00255-9.
[47] Gao L, Long H, Shen J, Yu G, Liao MN, Yin Y. Optical dating of Holocene tidal deposits from the southwestern coast of the South Yellow Sea using different grain-size quartz fractions. J Asian Earth Sci. 2017;135:155–65. doi: 10.1016/j.jseaes.2016.12.036.
[48] Gao L, Long H, Shen J, Yu G, Yin Y. High-resolution OSL dating of a coastal sediment sequence from the south yellow sea. Geochronometria. 2016;43:143–54. doi: 10.1515/geochr-2015-0044.
[49] Lu HY, An ZS. Paleoclimatic significance of grain size of loess-palaeosol deposit in Chinese Loess Plateau. Sci China Earth Sci. 1998;41(6):626–31. doi: 10.1007/BF02878745.
[50] Paterson GA, Heslop D. New methods for unmixing sediment grain size data. Geochem Geophys Geosys. 2015;16(12):4494–506. doi: 10.1002/2015GC006070.
[51] Nottebaum V, Stauch G, Hartmann K, Zhang JR. Unmixed loess grain size populations along the northern Qilian Shan (China): Relationships between geomorphologic, sedimentologic and climatic controls. Quat Int. 2015;372:151–6. doi: 10.1016/j.quaint.2014.12.071.
[52] Zhang XD, Ji Y, Yang ZS, Wang ZB, Liu DS, Jia PM. End member inversion of surface sediment grain size in the South Yellow Sea and its implications for dynamic sedimentary environments. Sci China Earth Sci. 2016;59:258–67. doi: CNKI:SUN:JDXG.0.2016-02-004.
[53] Hong YT, Hong B, Lin QH. Correlation between Indian Ocean summer monsoon and North Atlantic climate during the Holocene. Earth Planet Sci Lett. 2003;211:371–80. doi: 10.1016/S0012-821X(03)00207-3.
[54] Dykoski CA, Edwards RL, Cheng H, Yuan DX, Cai YJ, Zhang ML, et al. A high-resolution, absolute-dated Holocene and deglacial Asian Monsoon record from Dongge Cave, China. Earth Planet Sci Lett. 2006;233:71–86. doi: 10.1016/j.epsl.2005.01.036.
[55] Ji JF, Shen J, Balsam W. Asian monsoon oscillations in the northeastern Qinghai–Tibet Plateau since the late glacial as interpreted from visible reflectance of Qinghai Lake sediments. Earth Planet Sci Lett. 2005;233:61–70. doi: 10.1016/j.epsl.2005.02.025.
[56] Wang Y. The environment and resource of radial sand ridge field in the South Yellow Sea. China: Ocean Press; 2014. p. 1–39 (in Chinese).
[57] Zhou WJ, Head MJ, Deng L. Climate changes in northern China since the late Pleistocene and its response to global change. Quat Int. 2001;83–85:285–92. doi: 10.1016/S1040-6182(01)00046-5.

[58] Yu G, Xue B, Sun X. Reconstruction of Asian palaeomonsoon patterns in China over the last 40k years: a synthesis. Quat Res (Daiyongki-Kenkyuu). 2002;41(1):23–33. doi: 10.4116/jaqua.41.23.
[59] Van Geel B, Buurman J, Waterbolk HT. Archaeological and palaeoecological indications of an abrupt climate change in the Netherlands, and evidence for climatological teleconnections around 2650 BP. J Quat Sci. 1996;11:451–60. doi: 10.1002/(SICI)1099-1417(199611/12)11:6<451:AID-JQS275>3.0.CO;2-9.
[60] Hong YT, Jiang HB, Liu TS, Zhou LP, Beer J, Li HD, et al. Response of climate to solar forcing recorded in a 6000-year d18O time-series of Chinese peat cellulose. Holocene. 2000;10:1–7. doi: 10.1191/095968300669856361.
[61] Liu KB, Sun S, Jiang X. Environmental change in the Yangtze River Delta since 12,000 years B.P. Quat Res. 1992;38:32–45. doi: 10.1016/0033-5894(92)90028-H.
[62] Jia M, Zhang D, Cheng G, Wang H. First discovery of ice wedges in northeast China. J Glaciol Geocryol. 1987;9:257–60 (in Chinese).
[63] Peng H, Cheng G. The ice wedges in Da Hinggan Ling prefecture, northeast China and their palaeoclimatic significance. Proceedings of fourth national conference on glaciology and geocryology (selection). Beijing: Science Press; 1990. p. 9–16 (in Chinese).
[64] Jiang Q, Piperno DR. Environmental and archaeological implications of a Late Quaternary palynological sequence, Poyang Lake, Southern China. Quat Res. 1999;52:250–8. doi: 10.1006/qres.1999.2070.
[65] Yi SH, Saito Y, Yang DY. Palynological evidence for Holocene environmental change in the Changjiang (Yangtze River) Delta, China. Palaeogeogr Palaeoclimatol Palaeoecol. 2006;241:103–17. doi: 10.1016/j.palaeo.2006.06.016.
[66] Chu KC. A preliminary study on the climatic fluctuations during the last 5,000 years in China. Sci Sin. 1973;16:226–56.
[67] Sakaguchi Y. Warm and cold stages in the past 7600 years in Japan and their global correlation. Bull Dep Geogr Univ Tokyo. 1983;15:1–31.
[68] Jian Z, Wang P, Saito Y, Wang J, Pflaumann U, Oba T, et al. Holocene variability of the Kuroshio current in the Okinawa Trough, northwestern Pacific Ocean. Earth Planet Sci Lett. 2000;194:305–19. doi: 10.1016/S0012-821X(00)00321-6.
[69] Chen R, Shen J, Li CH, Zhang EL, Sun WW, Ji MM. Mid- to late-Holocene East Asian summer monsoon variability recorded in lacustrine sediments from the Jingpo Lake. Northeastern China Holocene. 2015;25:454–68. doi: 10.1177/0959683614561888.
[70] Gao S, Collins MB. Holocene sedimentary systems on continental shelves. Mar Geol. 2014;352:268–94. doi: 10.1016/j.margeo.2014.03.021.
[71] Laskar J, Robutel P, Joutel F, Gastuneau M, Correia ACM, Levrard B. A long-term numerical solution for the insolation quantities of the Earth. Astron Astrophys. 2004;428:261–85. doi: 10.1051/0004-6361:20041335.